International Journal of Bifurcation and Chaos, Vol. 17, No. 6 (2007) 2097–2108

LABYRINTH CHAOS

J. C. SPROTT
Department of Physics, University of Wisconsin, 1150 University Avenue, Madison, WI 53706, USA

KONSTANTINOS E. CHLOUVERAKIS
Department of Informatics and Telecommunications, University of Athens, Athens 15784, Greece

Received July 24, 2006; Revised August 29, 2006

A particularly simple and mathematically elegant example of chaos in a three-dimensional flow is examined in detail. It has the property of cyclic symmetry with respect to interchange of the three orthogonal axes, a single bifurcation parameter that governs the damping and the attractor dimension over most of the range 2 to 3 (as well as 0 and 1) and whose limiting value $b = 0$ gives Hamiltonian chaos, three-dimensional deterministic fractional Brownian motion, and an interesting symbolic dynamic.

Keywords: Attractor; multistability; diffusion; symbolic dynamics.

1. Introduction

René Thomas [1999] has proposed a particularly simple and mathematically elegant three-dimensional flow of the form

$$\begin{aligned} \dot{x} &= \sin y - bx \\ \dot{y} &= \sin z - by \\ \dot{z} &= \sin x - bz \end{aligned} \tag{1}$$

where the overdot denotes a time derivative. The system is representative of a large class of autocatalytic models that occur frequently in chemical reactions [Ramussen *et al.*, 1990], ecology [Deneubourg & Goss, 1989], and evolution [Kauffman, 1993]. The system is cyclically symmetric in the variables x, y, and z and is governed by a single parameter b that can be considered as a frictional damping for a particle moving in a three-dimensional lattice (or "labyrinth") under the influence of some external source of energy or other equivalent resource. In this paper, we examine the details of this system including its route to chaos, attractor dimension, multistability, chaotic diffusion, and symbolic dynamics. The system is of interest and importance because it provides an example of a system whose attractor can be tuned to almost any dimension in the range of 2 to 3 (as well as 0 and 1) by a single parameter and that has the rare quality of undergoing a continual transition from a chaotic dissipative system to a chaotic conservative system, albeit with embedded periodic windows. The conservative limit provides an elegant example of three-dimensional fractional Brownian motion in a purely deterministic system with a simple but interesting symbolic dynamic.

2. Route to Chaos

The parameter b provides a means to explore the route from a stable equilibrium to chaos and finally into the chaotic Hamiltonian regime. For $b > 1$, there is a single stable equilibrium at the origin ($x^* = y^* = z^* = 0$) whose eigenvalues λ_i satisfy the characteristic equation $(\lambda + b)^3 = 1$ with roots $\lambda_1 = 1 - b$ and $\lambda_{2,3} = -b - (1/2) \pm (\sqrt{3}/2)i$. The corresponding Lyapunov exponents are given by the

real parts of the eigenvalues, and they sum to $-3b$ as expected from the trace of the Jacobian matrix. For $b > 1$, the origin is a spiral node.

At $b = 1$, the equilibrium at the origin becomes unstable, and a pair of new stable symmetric equilibria are born in a pitchfork bifurcation with $x^* = y^* = z^* = \sin x^*/b$ or $x^* \cong \sqrt{6(1-b)}$ with eigenvalues that satisfy $(\lambda+b)^3 = \cos^3 x^*$. Setting $c = \cos x^*$ gives $\lambda_1 = c-b$ and $\lambda_{2,3} = -b-(c/2)\pm(\sqrt{3}c/2)i$ for $c > 0$ or $b > 2/\pi = 0.636619772\ldots$. At $b = 2/\pi$, the three Lyapunov exponents are equal ($\lambda_i = -2/\pi$), and the complex eigenvalues thereafter become dominant (have the least negative real parts).

As b is decreased further, the real part of these eigenvalues reaches zero in a Hopf bifurcation at $b = -c/2$ or $\tan x^* = -x^*/2$, whose solution by Newton's method is $x^* = 2.28892972810340436\ldots$ which occurs at $b = 0.32899010224273929\ldots$ with an imaginary part of $\omega = 0.56982757227170410\ldots$. The lone nonzero Lyapunov exponent has a value of $\lambda_3 = -3b = -0.986970306728218\ldots$ at the Hopf bifurcation. Thereupon a stable limit cycle is born, and the three variables take on different periodic values. These results are summarized in Fig. 1, which shows the Kaplan–Yorke dimension [Kaplan & Yorke, 1979] and the spectrum of Lyapunov exponents [Wolf *et al.*, 1985] from which it was determined over a range of $1.1 \geq b \geq 0$.

The range from the onset of a limit cycle at $b = 0.32899010224273929\ldots$ to the point where chaos becomes well established at $b \sim 0.11$ is very dynamically rich as shown in Fig. 2. The limit cycle first grows in size and then undergoes a succession of period-doubling bifurcations, culminating in a band of chaos that onsets around $b = 0.208186$. The resulting strange attractor then grows in size, albeit with embedded periodic windows, until an interior crisis occurs at $b \sim 0.18$, whereupon a new stable limit cycle is born. Thereafter follows a succession of similar crises, giving rise to more complicated limit cycles, culminating in bands of chaos, until chaos becomes dominant at $b \sim 0.11$.

The range from $b = 0.11$ to $b = 0$ is relatively well-behaved, with chaos dominating and a strange attractor whose dimension gradually increases from 2 to 3, but with embedded windows where limit cycles of various periods occur as shown in Fig. 3. Also shown in Fig. 3 is the value of the correlation dimension with error bars for specific values of b as calculated by the extrapolation method of Sprott and Rowlands [2001]. The correlation dimension tracks the Kaplan–Yorke dimension but

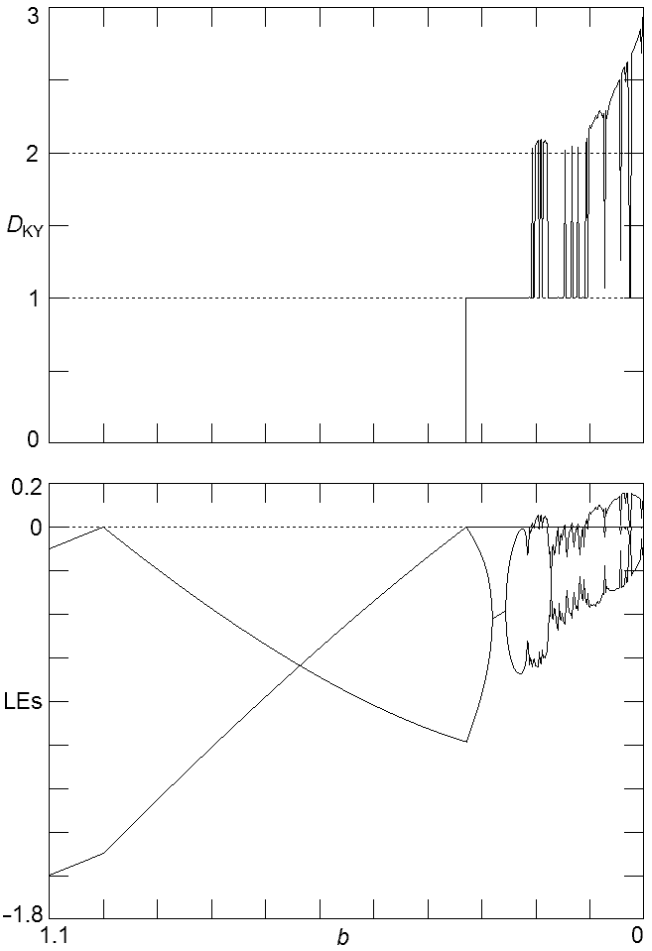

Fig. 1. Kaplan–Yorke dimension and Lyapunov exponents versus b showing the route to chaos.

systematically lower as expected for an attractor is with nonuniform measure. The reasonably smooth increase in dimension from 2 to 3 is unusual and makes this system good for studies in which the attractor dimension is an important parameter. The Lyapunov exponents in the limit of $b = 0$ are approximately $(0.09202, 0, -0.09202)$, and the Kaplan–Yorke dimension is exactly 3.0. The correlation dimension is 2.837 ± 0.173.

Figure 4 shows a cross-section of the attractor in yz-space at $x = 0$ for four values of b. The axes are -20 to 20 for each case. The plots suggest a highly nonuniform measure and a variation in local dimension across the attractor, as well as the expansion of the attractor with decreasing b. Also evident, especially in the plot for $b = 0.01$, are vertical stripes at $y = \pm m\pi$, where $m = 0, 1, 2, \ldots$, which represent the nullclines for which $\dot{x} = 0$ at $x = 0$. For the four cases in Fig. 4 with $b = (0.1, 0.05, 0.02, 0.01)$, the

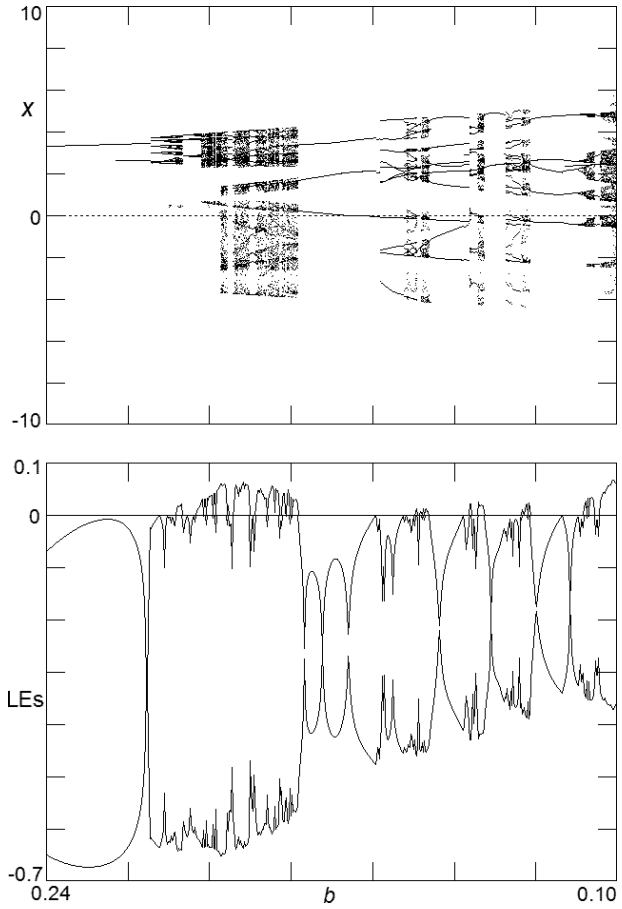

Fig. 2. Bifurcation diagram (local maximum of x) and Lyapunov exponents versus b showing the route to chaos in greater detail.

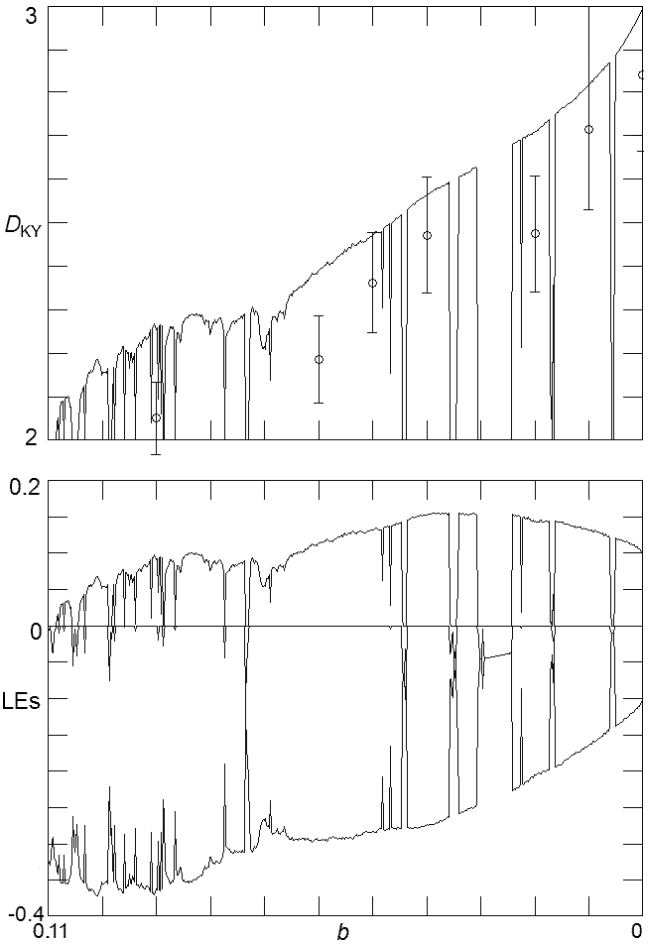

Fig. 3. Kaplan–Yorke dimension and Lyapunov exponents versus b showing the route to chaos. In the upper plot, the circles with error bars are values of the correlation dimension.

Kaplan–Yorke dimensions are $D_{\mathrm{KY}} \cong (2.155, 2.468, 2.708, 2.815)$, and the corresponding largest Lyapunov exponents are $\lambda_1 \cong (0.055, 0.132, 0.145, 0.132)$.

In calculating these attractors and their spectra of Lyapunov exponents, initial conditions are chosen randomly in the range of 0 to 1 and are not critical. However, there is a set of measure zero of initial conditions with $x(0) = y(0) = z(0)$ for which the three variables remain identical for all time, and the system behaves like a one-dimensional system with stable equilibria (point attractors) at $x^* = y^* = z^*$, that satisfy $\sin x^* = bx^*$, whose solution for $b \ll 1$ is $x^* \cong \pm n\pi/(b+1)$, where n is an odd integer.

Another way to view the expansion of the attractor with decreasing b is to plot the standard deviation of the trajectory from the origin

$$\sigma = \sqrt{\lim_{T\to\infty} \frac{1}{T} \int_0^T (x^2 + y^2 + z^2) dt} \qquad (2)$$

along with the kurtosis [Press *et al.*, 1992]

$$k = \lim_{T\to\infty} \frac{1}{T\sigma^4} \int_0^T \left(x^2 + y^2 + z^2\right)^2 dt - 3 \qquad (3)$$

averaged along the trajectory as shown in Fig. 5. The kurtosis is defined such that a value of $k = 0$ represents a normal (Gaussian) distribution, and the calculated negative values indicate that the distribution is somewhat platykurtic (the tail of the distribution is truncated relative to a Gaussian). The standard deviation (ignoring the periodic windows) scales with b roughly as $\sigma \approx 1.5/\sqrt{b}$. By the ergodic hypothesis [Ruelle, 1976], these time averages are identical to the ensemble averages over many initial conditions and coarsely reflect the natural measure on the attractor apart from the fine-scale fractal structure.

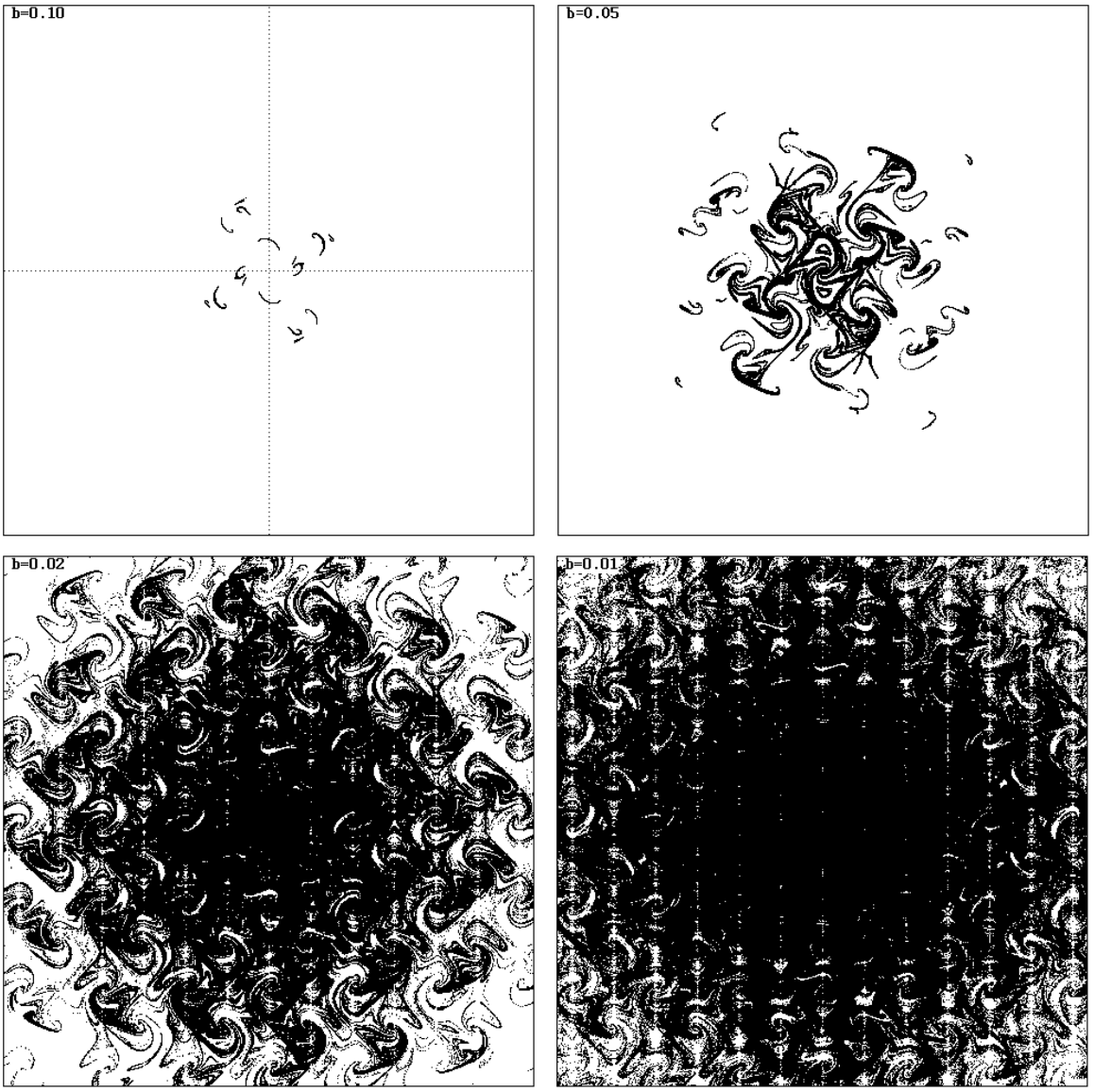

Fig. 4. Cross-section of the attractor in yz-space at $x = 0$ for four values of b. The axes are -20 to 20 for each case.

3. Multiple Attractors and Global Bifurcations

In the preceding discussion and figures, the value of b was slowly decreased without altering the initial conditions, and hence the results represent only one route to chaos. The possibility of multiple attractors for a given b and hysteresis was not indicated, nor was there a clear distinction between local and global bifurcations.

To explore these issues, define a quantity r analogous to Eq. (2)

$$r = \frac{\sqrt{b}}{1.5}\sqrt{\lim_{T\to\infty}\frac{1}{T}\int_0^T [(x-x_{\rm ref})^2 + (y-y_{\rm ref})^2 + (z-z_{\rm ref})^2]dt} \tag{4}$$

that has been multiplied by $\sqrt{b}/1.5$ to account for the increase in attractor size as b decreases and that has been offset from the origin along each axis to remove degeneracies resulting from the cyclic symmetry. In what follows, the offsets are taken as $x_{\rm ref} = \pi G$, $y_{\rm ref} = \pi G^2$ and $z_{\rm ref} = \pi G^3$, where G is

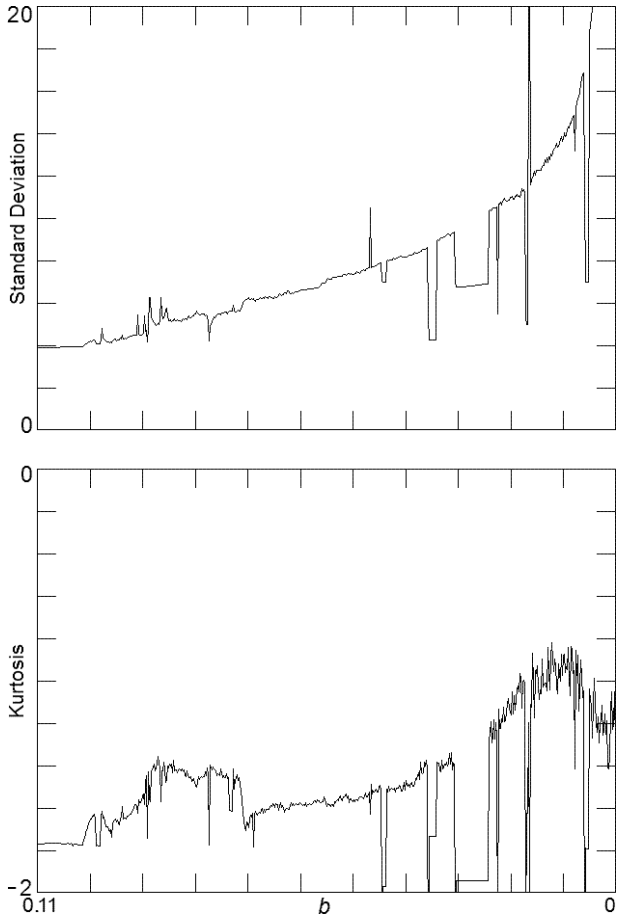

Fig. 5. Standard deviation and kurtosis for the excursion of the trajectory from the origin for the attractors as a function of b.

the golden mean, $G = (\sqrt{5} - 1)/2 = 0.61803398\ldots$. Then make a plot of r versus b for many different random initial conditions uniform in the range $-\pi$ to π for each value of b. Since two different attractors are very unlikely to have identical values of r, the plot will show the values of b for which there are multiple coexisting attractors along with the bifurcations where the attractors appear, disappear or undergo a sudden change in size or position.

Such a plot is shown in Fig. 6 where 50 different initial conditions were used for each of the 600 values of b, with each case iterated 2×10^5 times using a fourth-order Runge–Kutta method with a fixed step size of 0.05 with the first 10% of the points ignored to allow the trajectory to reach the attractor. Most values of b apparently admit only a single attractor, which must itself be cyclically symmetric in the three variables, but there are values for which up to six distinct attractors are evident. The chaotic regions have a band of values, indicating a rather slow convergence especially at the embedded

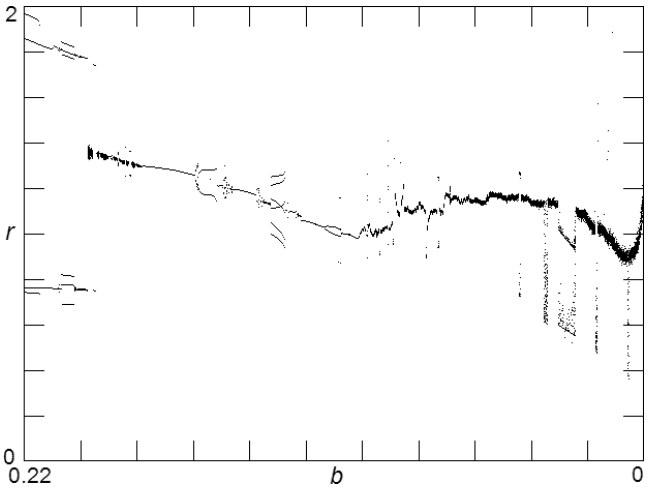

Fig. 6. Plot showing regions of multiple coexisting attractors as a function of b.

periodic windows, where transient chaos and intermittency are common.

Figure 7 shows cases in which there are four ($b = 0.220$), six ($b = 0.204$), three ($b = 0.173$), and six ($b = 0.131$) coexisting limit cycles, respectively. The linking property of these loops is an interesting issue not explored here. Lest one concludes that coexisting attractors exist only for limit cycles, Fig. 8 shows a ($b = 0.203$) case in where there are six coexisting strange attractors. However, it is generally the case that slightly beyond the onset of chaos, these independent attractors undergo a crisis and merge into a single strange attractor in an attractor-merging global bifurcation [Grebogi *et al.*, 1983].

4. Conservative Case

The remainder of the paper will be concerned with the limit of $b = 0$, for which the system in Eq. (1) has no dissipation, and where the trajectory wanders chaotically throughout the entire xyz space except for about 1.67% of the space where the trajectory drifts out parallel to one of the three axes with a constant average velocity of about 0.41 while executing periodic oscillations with a period of about 15.2 in a plane perpendicular to that axis. There are infinitely many equilibria at $x^* = \pm l\pi$, $y^* = \pm m\pi$, $z^* = \pm n\pi$, where l, m, and n are arbitrary integers. The system can also be considered as a 3-torus with period 2π in each direction and only eight equilibria.

Figure 9 shows a yz cross-section of the trajectory (mod 2π) in the (x mod 2π) $= 0$ plane for a single trajectory that starts in the chaotic sea.

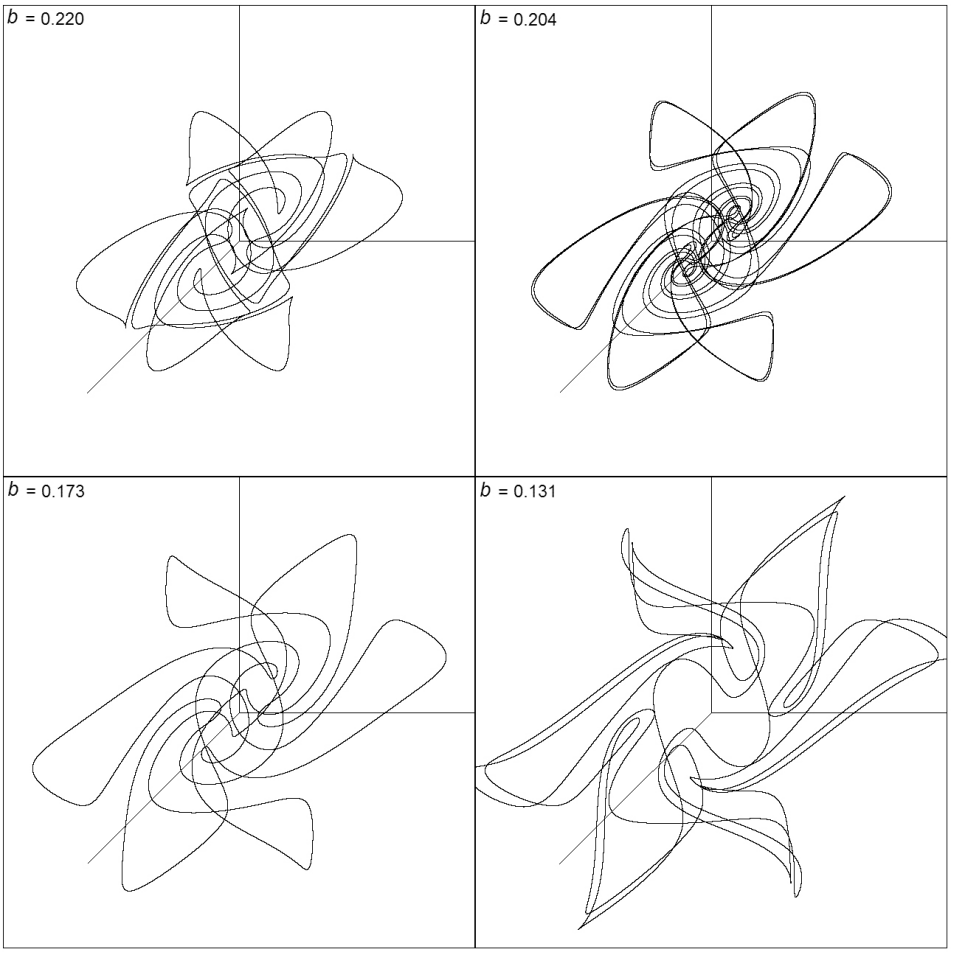

Fig. 7. Multiple coexisting limit cycles.

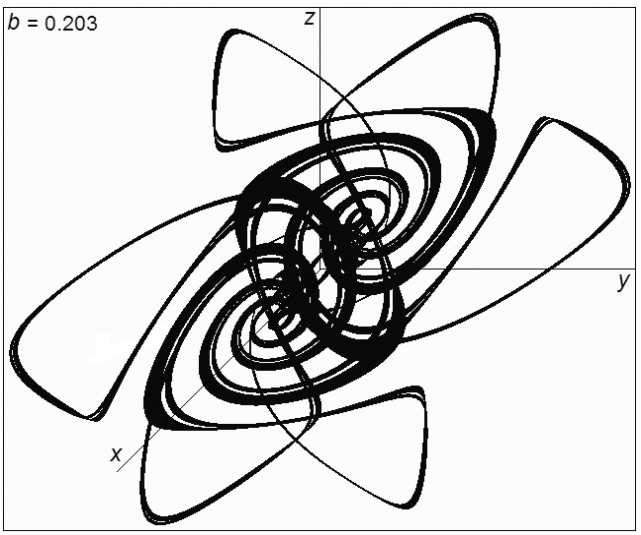

Fig. 8. Six coexisting strange attractors at $b = 0.203$.

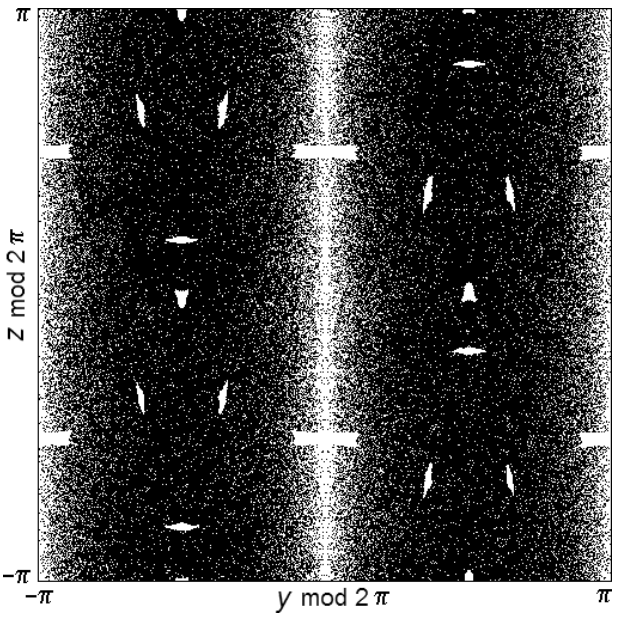

Fig. 9. Cross-section of the chaotic sea at (x mod 2π) = 0 for the conservative case with $b = 0$.

The trajectory is ergodic and eventually comes arbitrarily close to every point in the sea. The nullclines, where the trajectory has only a y-component, are evident as vertical stripes at $y = 0$ and $y = \pm\pi$, and the 20 loss regions in each cell are indicated by the empty islands in the sea, accounting for about 1.9% of the cross-sectional area, surrounded by KAM surfaces [Arnold, 1978]. These loss regions are actually intertwined helical ribbon structures as shown stereographically in Fig. 10, some of which are tangent to the $x = 0$ plane, explaining why the area in this plane (1.9%) is greater than their volume (1.67%). These structures are of two types, one passing through the points $(x, y, z) = (0, 0, \pm\pi/2)$ and the other passing through the points $(x, y, z) = (0, \pm\pi/2, \pi)$ and their cyclic permutations, giving twelve separate ribbons, two of which lead to drifts in each of the six directions $\pm x$, $\pm y$, and $\pm z$. In addition to the intersections of these ribbons with the $x = 0$ plane at 0, $\pm\pi/2$, and π, there are other intersections at approximately $\pm 0.19\pi$, $\pm 0.36\pi$, $\pm 0.64\pi$, and $\pm 0.81\pi$, although not in all combinations. Figure 11 shows a cross-section in the yz-plane of one of these ribbons whose center is at

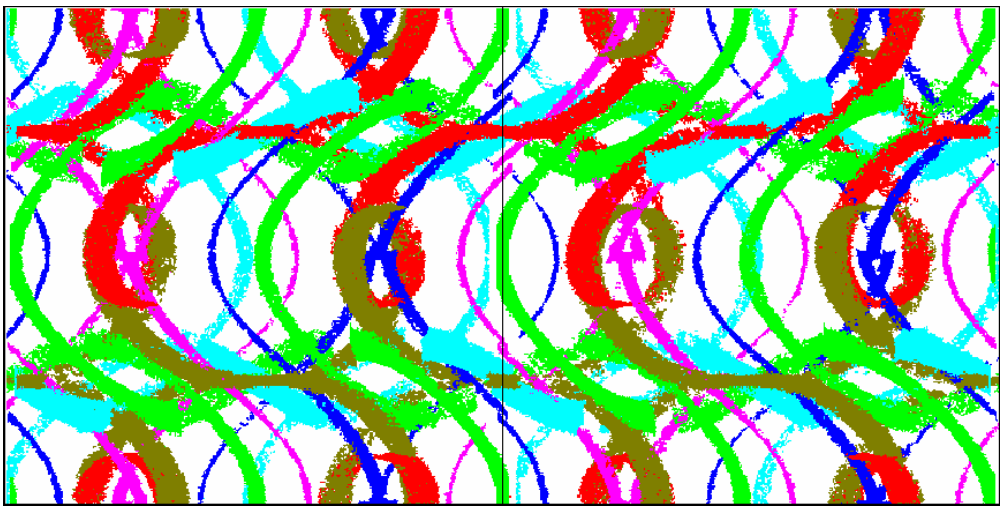

Fig. 10. Stereogram showing the regions where quasiperiodic trajectories occur for $b = 0$. The view is looking down along the x-axis, and the different colors denote the six directions in which trajectories drift.

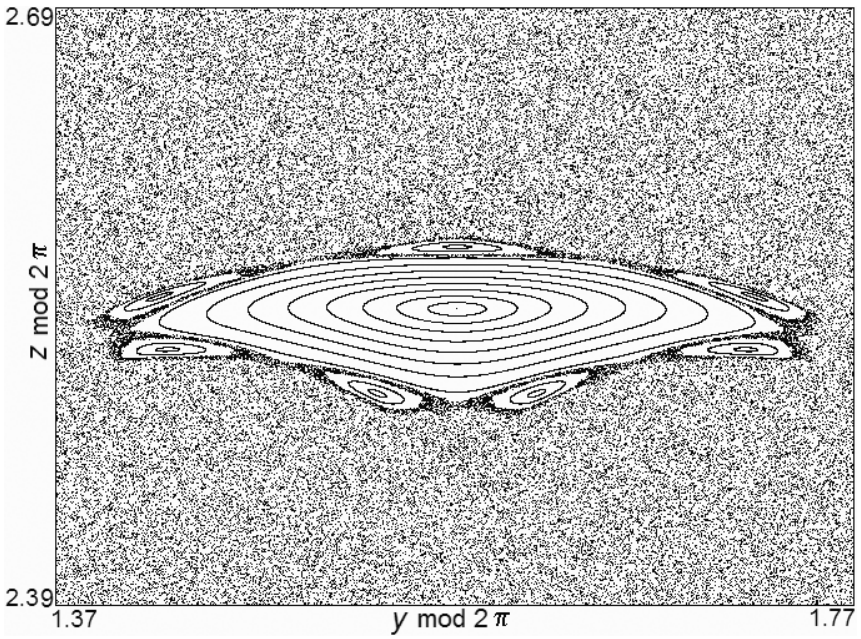

Fig. 11. Cross-section at $(x \bmod 2\pi) = 0$ showing the quasiperiodic orbits for $b = 0$ surrounded by a KAM surface.

$(0,\ \pi/2,\ \sim 0.808219\pi)$, near the edge of which is a chain of seven smaller islands. The quasiperiodic regions are invariant 2-tori embedded in the hypersurface of a 3-torus.

5. Deterministic Fractional Brownian Motion

For the conservative case ($b = 0$), the trajectory wanders ergodically and time-reversibly throughout the entire three-dimensional space except for the small quasiperiodic regions. The equilibrium density $f(x, y, z)$ in this chaotic sea is given by

$$\frac{df}{dt} = \frac{\partial f}{\partial x}\frac{dx}{dt} + \frac{\partial f}{\partial y}\frac{dy}{dt} + \frac{\partial f}{\partial z}\frac{dz}{dt}$$

$$= \frac{\partial f}{\partial x}\sin y + \frac{\partial f}{\partial y}\sin z + \frac{\partial f}{\partial z}\sin x = 0 \quad (5)$$

whose solution is $f(x, y, z) =$ constant. Equivalently, note that the divergence of the flow

$$\nabla \cdot \vec{v} = \frac{\partial}{\partial x}\sin y + \frac{\partial}{\partial y}\sin z + \frac{\partial}{\partial z}\sin x \equiv 0 \quad (6)$$

is identically zero, which means that the flow is incompressible and hence of constant density throughout the ergodic region. Given the uniform measure, it is simple to calculate the root-mean-square speed:

$$v_{rms} = \sqrt{\overline{\sin^2 y} + \overline{\sin^2 z} + \overline{\sin^2 x}} = \sqrt{\frac{3}{2}}$$

$$= 1.2247449\ldots \quad (7)$$

each component of which is $1/\sqrt{2} = 0.7071068\ldots$.

However, the approach to this equilibrium is by way of a diffusion, reminiscent of Brownian motion, but in a purely deterministic system. The trajectory for one such typical case is shown in Fig. 12 along with a typical quasiperiodic trajectory in red for an initial condition of $(0,\ 0,\ \pi/2)$. For a collection of 5×10^6 initial conditions that start at random positions near the origin, the probability distribution function along each axis after a time lapse of 4×10^3 is shown in Fig. 13. Also shown in the figure in red

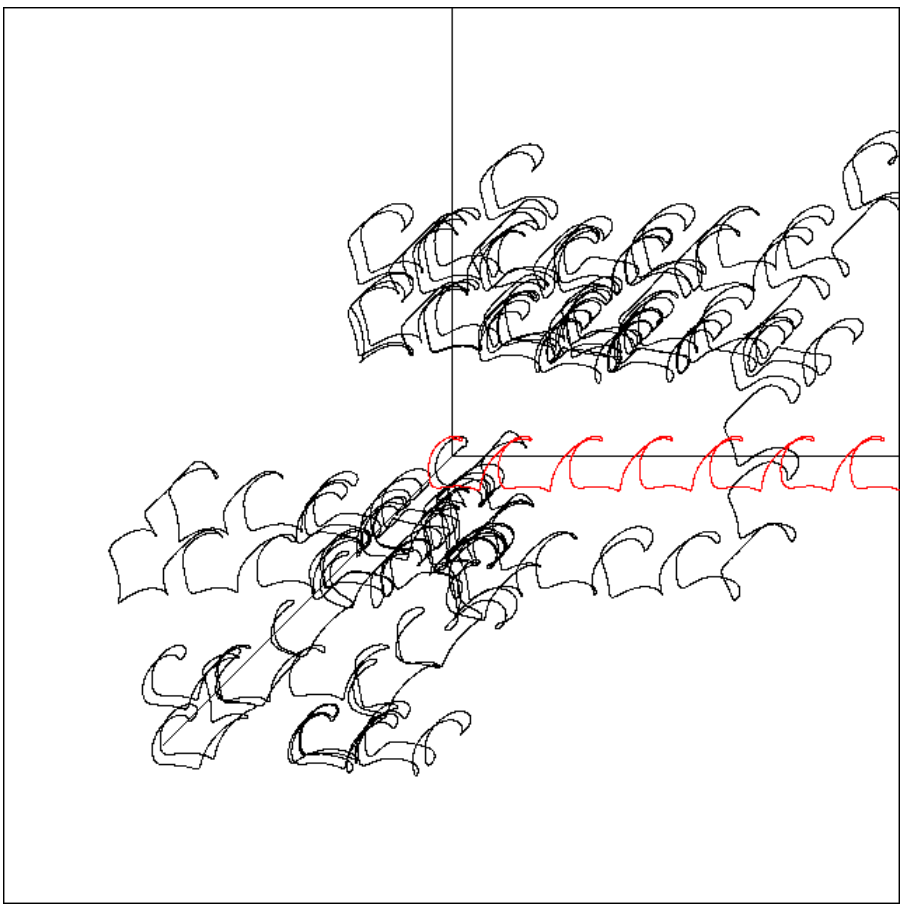

Fig. 12. Brownian motion of a trajectory in the chaotic sea (black) along with a quasiperiodic trajectory (red).

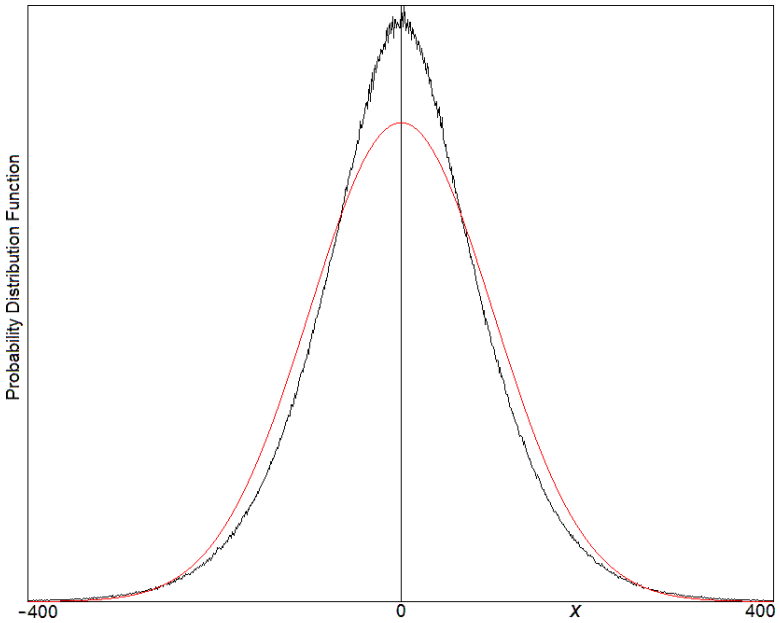

Fig. 13. Probability distribution function of x for 5×10^6 initial conditions near the origin after a time of 4×10^3. The red curve is a Gaussian distribution with the same standard deviation and area.

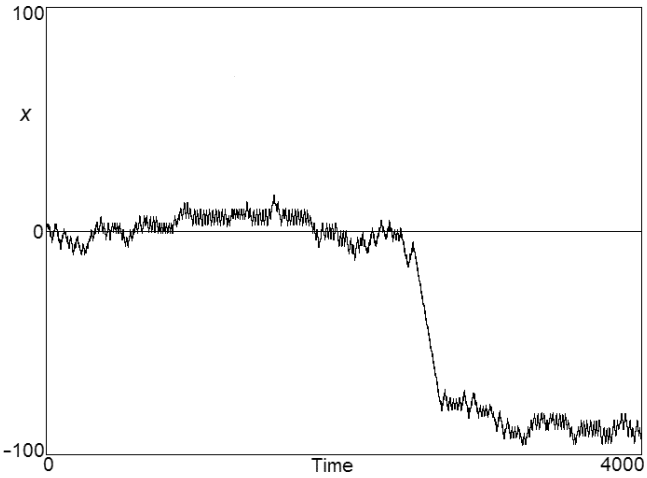

Fig. 14. Projection of the trajectory onto the x-axis showing an example of intermittency where the trajectory approaches the quasiperiodic region with initial conditions $(0.05, 0.09, 0.05)$.

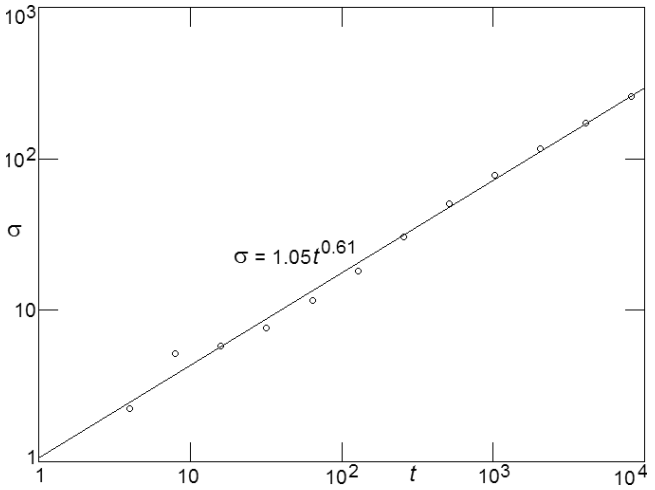

Fig. 15. Standard deviation of 1.5×10^6 trajectories starting near the origin versus time.

is a Gaussian distribution with the same standard deviation ($\sigma \cong 98.3$) and area. The observed distribution is leptokurtic (fat-tailed) with a kurtosis of $k \cong 9.8$. The enhanced tail of the distribution is due to chaotic trajectories that occasionally approach the quasiperiodic regions and travel great distances parallel to one of the axes before resuming their random walk. This is a form of intermittency, a typical example of which is shown in Fig. 14. There is a time at which the trajectory makes a large excursion in the x-direction, but there are other times evident in the figure where x is nearly periodic and the trajectory makes large excursions in either y or z.

Despite the non-Gaussian nature of the distribution function, it is possible to plot the standard deviation (the average value of $\sqrt{x(t)^2 + y(t)^2 + z(t)^2}$) versus time for a random collection of initial conditions near the origin. Figure 15 shows such a plot for 1.5×10^6 initial conditions uniform over a cube centered on the origin and extending from -0.1 to 0.1 along

each axis. The slope of the least-squares fitted curve (0.61) indicates that the motion is not purely Brownian (for which the slope would be 0.5), but rather is an example of fractional Brownian motion [Mandelbrot, 1983] in which the trajectory exhibits persistence (positive correlation) and preferentially continues in the direction in which it was previously headed. This slope is somewhat smaller than the value of 0.73 reported earlier [Sprott, 2003] because it discounts those initial conditions for which the trajectory drifts uniformly parallel to one of the axes.

From the best fit linear regression of log σ versus log t given by $\sigma = 1.05t^{0.61}$ and assuming $\sigma = (t/\tau)^H d$, where τ is an effective collision time and d is an effective mean free path with $d/\tau = v$ given by Eq. (7), one obtains $\tau = (1.05/1.22)^{2.56} \cong 0.68$ and $d = 1.22 \times 0.68 \cong 0.83$, which is somewhat smaller than the lattice size of 2π. The quantity H (= 0.61 in this case) is called the Hurst exponent [Hurst *et al.*, 1965].

An alternate calculation of the Hurst exponent uses a single trajectory followed for a very long time with the rescaled range R/S plotted versus time on a log–log plot, the slope of which is H [Feder, 1988]. The range R is the maximum excursion from the starting point, and S is the average step size (approximately the mean free path, d), which does not depend on time. Hence it suffices just to plot log R versus log t as shown in Fig. 16(a), where the slope of the best fit straight line is $H = 0.62$, in good agreement with the value of 0.61 obtained from Fig. 15. In Fig. 16 the initial condition was taken as $(0.2, 0, 0)$, and the trajectory was followed for a time of 10^9 with a step size of 0.05.

Also shown in Fig. 16(b) is the autocorrelation function

$$C(\tau) = \frac{\int_\tau^\infty \dot{x}(t)\dot{x}(t-\tau)dt}{\int_\tau^\infty \dot{x}(t)^2 dt} \qquad (8)$$

for the same trajectory showing the short-term correlation and mild persistence ($C(\tau) > 0$). The autocorrelation function is the Fourier transform of the power spectral density (PSD) [Couch, 2001] and was performed on the time derivative of x rather than x itself because the mean of $\dot{x}$ is more nearly zero and the PSD is more nearly flat (white). In fact, for a power-law spectrum $1/f^\alpha$ with a Hurst exponent H, the slope of the PSD for $x(t)$ is expected

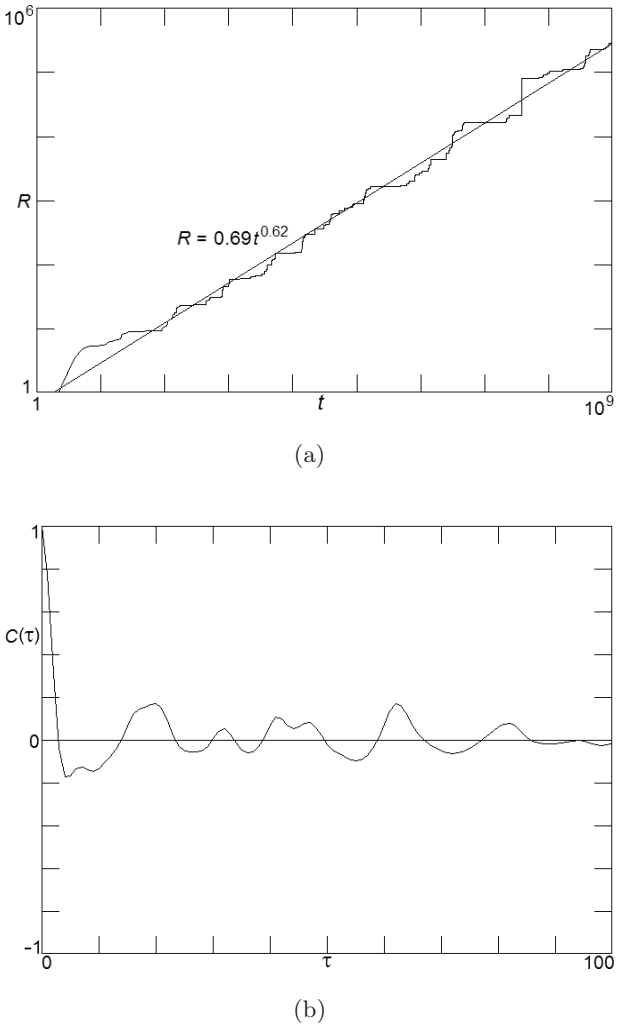

Fig. 16. (a) Range versus time, and (b) autocorrelation function of $\dot{x}$ versus delay for an initial condition of $(0.2, 0, 0)$.

to be $\alpha = 2H + 1$ [Tsonis, 1992], and for $\dot{x}(t)$ is $2H - 1 = 0.22$ for $H = 0.61$.

6. Symbolic Dynamics

An alternate representation of the dynamics exploits the 2π periodicity of the lattice along each of the three axes which divides the space into an infinite number of cubes. Each such cube can be subdivided into eight equal cubic chambers characterized by the signs of $\dot{x}$, $\dot{y}$, and $\dot{z}$. Thus the trajectory sequentially visits neighboring chambers, labeled A through H, with A being the one with all derivatives positive, B being the one with $\dot{x}$ negative and the others positive, C being the one with $\dot{y}$ negative and the others positive, D being the one with both $\dot{x}$ and $\dot{y}$ negative with $\dot{z}$ positive, and so forth. Thus the trajectory can be represented as an infinite symbol sequence with an 8-letter

alphabet. With this convention, the quasiperiodic trajectory starting at $(0, 0, \pi/2)$ has the periodic sequence ACGEFHDBACGEFHDB..., and the one starting at $(0, \pi/2, \pi)$ has the periodic sequence CDBAEFHGCDBAEFHG.... Note that these trajectories visit all eight chambers before repeating.

The trajectory in the chaotic sea has a nonrepeating sequence, a typical portion of which is AEFBACDHFBAEGCDBAEFBDHGCAEGCDHFBDHGC.... From the symmetry of the system, we expect and observe all symbols to occur with equal probability (1/8). However, such is not the case for all 64 pairs of sequential symbols. Instead, each symbol can be followed by only three others with equal probability (1/3), despite the fact that each chamber has six neighbors. Thus only 24 of the possible 64 pairs occur. Furthermore, the symbol sequence is time-reversible in the sense that any segment of finite length will eventually occur with those symbols in the reversed order along the same trajectory. However, the trajectory has to leave a chamber by way of one of the two through which it did not enter, but with equal probability (1/2), so that, although the transitions AB and BA are both allowed, for example, the transitions ABA and BAB are not allowed. This behavior is summarized in Fig. 17 in which the symbols can be considered vertices of a cube whose edges represent the allowed transitions, with the trajectory entering along one edge and exiting with equal probability along one of the other two.

Another way to represent the dynamics is by way of an iterated function system [Barnsley, 1988] using eight affine transformations on the unit square, one corresponding to each symbol as follows:

$$\begin{aligned}
A: &\quad x \to \frac{x}{4}, && y \to \frac{y}{2} \\
B: &\quad x \to \frac{x}{4}, && y \to \frac{y+1}{2} \\
C: &\quad x \to \frac{x+1}{4}, && y \to \frac{y}{2} \\
D: &\quad x \to \frac{x+1}{4}, && y \to \frac{y+1}{2} \\
E: &\quad x \to \frac{x+2}{4}, && y \to \frac{y}{2} \\
F: &\quad x \to \frac{x+2}{4}, && y \to \frac{y+1}{2} \\
G: &\quad x \to \frac{x+3}{4}, && y \to \frac{y}{2} \\
H: &\quad x \to \frac{x+3}{4}, && y \to \frac{y+1}{2}
\end{aligned} \tag{9}$$

The transformations are performed in the order of the symbol sequence with an arbitrary initial

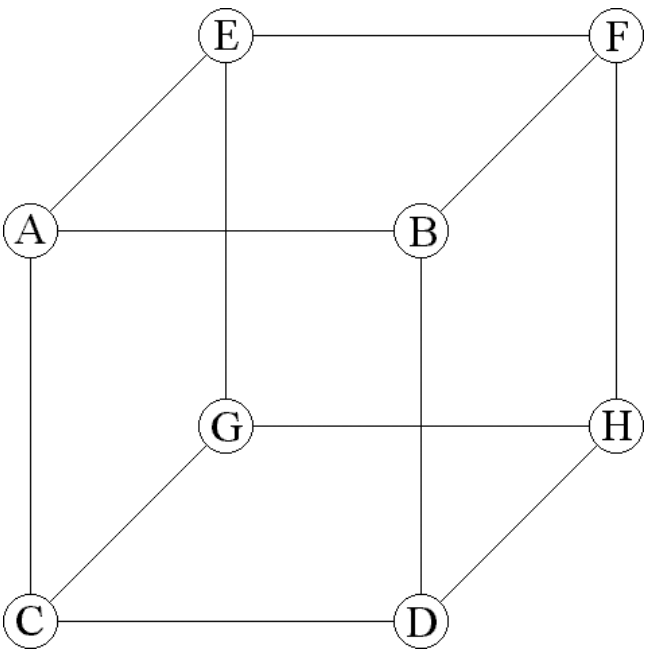

Fig. 17. Allowable transitions for symbolic sequence.

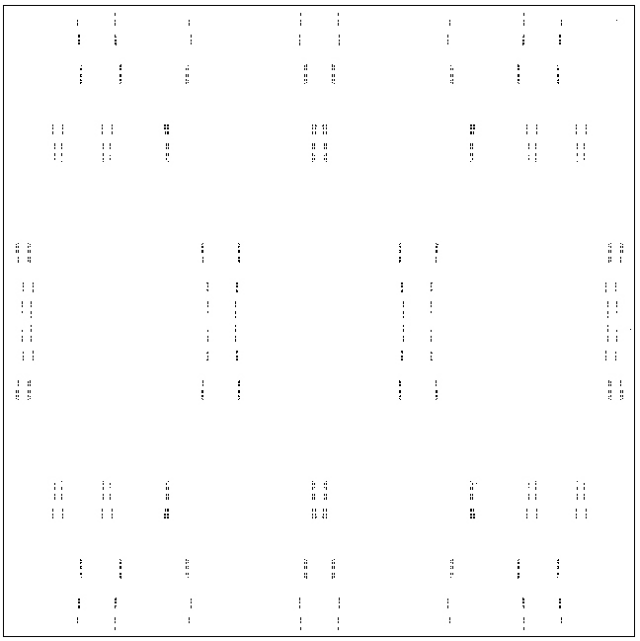

Fig. 18. Iterated function system representation of symbolic dynamic.

condition, here taken as $x = y = 0$, and the sequence of points is plotted in the xy-plane after discarding the first few iterates. A random sequence will fill in the unit square uniformly, and a periodic sequence will produce a finite collection of points [Peak & Frame, 1994]. The result for a trajectory in the chaotic sea with a sequence of 6×10^6 symbols is shown in Fig. 18. The fractal nature of the plot is a signature of chaos.

7. Conclusions

Despite its mathematical simplicity, the system of ordinary differential equations in Eq. (1) produces a surprisingly rich dynamic that can serve as a prototype for chaos studies. The system has a single parameter b that controls the damping and that is a natural bifurcation parameter for studying the route to chaos. As b approaches zero, the system smoothly and continuously transforms into a chaotic Hamiltonian system in which nearly all ($>98\%$) of the initial conditions ergodically explore the infinite chaotic sea with uniform measure. The approach to equilibrium is by way of fractional Brownian motion with a Hurst exponent of approximately 0.61 and a slightly leptokurtic distribution. An obvious extension of this work is to dimensions higher than three [Thomas *et al.* 2005], and that will be the subject of a forthcoming publication.

Acknowledgments

We are grateful to William Hoover for helpful discussions and to René Thomas for calling our attention to this system.

References

Arnold, V. I. [1978] *Mathematical Methods of Classical Mechanics*, 2nd edition (Springer, NY).

Barnsley, M. [1988] *Fractals Everywhere* (Academic Press, Boston).

Couch, L. W. [2001] *Digital and Analog Communications Systems*, 6th edition (Prentice Hall, Englewood Cliffs, New Jersey), pp. 406–409.

Deneubourg, J.-L. & Goss, S. [1989] "Collective patterns and decision-making," *Ethol. Ecol. Evol.* **1**, 295–312.

Feder, J. [1988] *Fractals* (Plenum, NY).

Grebogi, C., Ott, E. & Yorke, J. A. [1983] "Crises, sudden changes in chaotic attractors and transient chaos," *Physica D* **7**, 181–200.

Hurst, H. E., Black, R. P. & Simaika, Y. M. [1965] *Long-Term Storage*: *An Experimental Study* (Constable, London).

Kaplan, J. & Yorke, J. [1979] "Chaotic behavior of multidimensional difference equations," in *Functional Differential Equations and Approximations of Fixed Points*, Lecture Notes in Mathematics, Vol. 730, eds. Peitgen, H.-O. & Walther, H.-O. (Springer, Berlin), pp. 228–237.

Kauffman, S. [1993] *The Origins of Order* (Oxford University Press).

Mandelbrot, B. B. [1983] *The Fractal Geometry of Nature* (Freeman, San Francisco).

Peak, D. & Frame, M. [1994] *Chaos under Control: The Art and Science of Complexity* (Freeman, NY).

Press, W. H., Flannery, B. P., Teukolsky, S. A. & Vetterling, W. T. [1992] *Numerical Recipes*: *The Art of Scientific Computing*, 2nd edition (Cambridge University Press).

Rasmussen, S., Knudsen, C., Feldberg, R. & Hindsholm, M. [1990] "The coreworld: Emergence and evolution of cooperative structures in a computational chemistry," *Physica D* **42**, 111–134.

Ruelle, D. [1976] "A measure associated with Axiom A attractors," *Amer. J. Math.* **98**, 619–654.

Sprott, J. C. & Rowlands, G. [2001] "Improved correlation dimension calculation," *Int. J. Bifurcation and Chaos* **11**, 1861–1880.

Sprott, J. C. [2003] *Chaos and Time-Series Analysis* (Oxford University Press), pp. 196–198.

Thomas, R. [1999] "Deterministic chaos seen in terms of feedback circuits: Analysis, synthesis, 'labyrinth chaos'," *Int. J. Bifurcation and Chaos* **9**, 1889–1905.

Thomas, R., Basios, V., Eiswirth, M., Kruel, T. & Rössler, O. E. [2005] "Hyperchaos of arbitrary order generated by a single feedback circuit, and the emergence of chaotic walks," *Chaos* **14**, 669–674.

Tsonis, A. A. [1992] *Chaos*: *From Theory to Applications* (Plenum, NY).

Wolf, A., Swift, J. B., Swinney, H. L. & Vastano, J. A. [1985] "Determining Lyapunov exponents from a time series," *Physica D* **16**, 285–317.